Eur Radiol
DOI 10.1007/s00330-012-2508-0

MUSCULOSKELETAL

# Advanced MR methods at ultra-high field (7 Tesla) for clinical musculoskeletal applications

**Siegfried Trattnig · Štefan Zbýň · Benjamin Schmitt · Klaus Friedrich · Vladimir Juras · Pavol Szomolanyi · Wolfgang Bogner**

Received: 2 March 2012 / Revised: 2 May 2012 / Accepted: 4 May 2012


**Abstract**
*Objectives* This article provides an overview of the initial clinical results of musculoskeletal studies performed at 7 Tesla, with special focus on sodium imaging, new techniques such as chemical exchange saturation transfer (CEST) and T2* imaging, and multinuclear MR spectroscopy.
*Methods* Sodium imaging was clinically used at 7 T in the evaluation of patients after cartilage repair procedures because it enables the GAG content to be monitored over time. Sodium imaging and T2* mapping allow insights into the ultra-structural composition of the Achilles tendon and help detect early disease. Chemical exchange saturation transfer was, for the first time, successfully applied in the clinical set-up at 7 T in patients after cartilage repair surgery. The potential of phosphorus MR spectroscopy in muscle was demonstrated in a comparison study between 3 and 7 T, with higher spectral resolution and significantly shorter data acquisition times at 7 T.
*Results* These initial clinical studies demonstrate the potential of ultra-high field MR at 7 T, with the advantage of significantly improved sensitivity for other nuclei, such as $^{23}$Na (sodium) and $^{31}$P (phosphorus).
*Conclusions* The application of non-proton imaging and spectroscopy provides new insights into normal and abnormal physiology of musculoskeletal tissues, particularly cartilage, tendons, and muscles.
*Key Points*
- *7 T magnetic resonance provides significantly improved sensitivity for $^{23}$Na and $^{31}$P.*
- *Initial clinical studies have now demonstrated ultra-high field MR operating at 7 T.*
- *7 T provides new insights into normal and abnormal physiology of musculoskeletal tissues.*

**Keywords** Sodium MRI at 7 T · Cartilage · Tendon · CEST · Metabolic imaging

S. Trattnig (✉) · Š. Zbýň · B. Schmitt · K. Friedrich · V. Juras · P. Szomolanyi · W. Bogner
MR Centre—High Field MR, Department of Radiology, Medical University of Vienna/Vienna General Hospital, Waehringer Guertel 18-20, A-1090 Vienna, Austria
e-mail: siegfried.trattnig@meduniwien.ac.at

S. Trattnig
Austrian Cluster for Tissue Regeneration, Ludwig Boltzmann Institute for Experimental and Clinical Traumatology, Vienna, Austria

V. Juras · P. Szomolanyi
Department of Imaging Methods, Institute of Measurement Science, Slovak Academy of Sciences, Dúbravská cesta 9, Sk-84219 Bratislava, Slovakia

## Introduction

By the end of the 1990s, high-field MRI at 3 Tesla had become the benchmark for routine clinical applications, as well as for clinical MRI research. The clinical benefits of the signal-to-noise ratio (SNR) that is twice that of standard 1.5 T MR consist mainly of the combined morphological and functional high-field MR methods possible at this field strength, such as functional MR, metabolic imaging, and diffusion-weighted imaging [1].

The next important step was taken in the early 2000s [2–5] and involved increasing the MRI field strength by another factor of approximately two, and, presently, at least three major MR vendors provide commercial 7 T units for human clinical research under ethics board-approved

Published online: 12 June 2012

conditions. Approximately 10 years ago, there were fewer than five ultra-high-field MR installations in the world. During the last several years, the number of installations finalized or under preparation has increased to about 40 (0.2% of the total installation number). This rapid increase indicates the growing interest in ultra-high-field MRI in the bio-imaging community, brought to the fore by promising results with regard to morphological detail, as well as functional imaging capability [6–8].

Most clinical MR research centers operating at 7 T primarily focus on neuroradiological applications, with only a few sites performing whole-body clinical research at 7 T. This is because of the limited availability of suitable coils for 7 T, which must be transmit-and-receive coils, the higher B0 and B1 heterogeneity related to the ultra-high field, as well as safety issues, particularly the increased specific absorption rate, which is about 22 times higher at 7 T compared to 3 T.

In this review, we want to provide an overview of the initial clinical results of musculoskeletal studies performed at 7 T, with a special focus on sodium imaging, new techniques such as chemical exchange saturation transfer (CEST) and T2* imaging, and multinuclear metabolic imaging or MR spectroscopy (MRS) in tissues such as cartilage, tendons, and muscles.

## Sodium MRI at 7 T

### Sodium imaging of cartilage and cartilage repair

Proton MRI at ultra-high-field (7 T and above) MR systems poses various challenges, including radiofrequency power deposition, increased chemical shift, susceptibility artifacts, homogeneity of RF coils, and changes in relaxation times, compared to lower-field clinical MR systems. These problems are much less pronounced in nuclei with a low gyromagnetic ratio, such as sodium ($^{23}$Na). However, a 3.8-fold smaller gyromagnetic ratio, a lower resonance frequency ($^{23}$Na: 78.6 MHz vs. $^{1}$H: 297.2 MHz), a significantly shorter T2 relaxation time, and a lower concentration of sodium nuclei ($^{23}$Na: 300 mM vs. $^{1}$H: 110 M) result in sodium MR signal in articular cartilage that is 1/4,000–1/5,000 smaller than the proton MR signal. In order to achieve sufficiently high SNR (SNR>15), sodium MRI requires longer measurement times (15–40 min) and results in low-resolution images. Ultra-high-field MR systems can provide higher intrinsic $^{23}$Na SNR and/or higher spatial/temporal resolution and improved contrast in the image [9, 10]. The MR relaxation properties of sodium nuclei in biological systems are dominated by quadrupolar interactions and result in short longitudinal (T1) and transverse relaxation (T2) times. Transverse relaxation is characterised by biexponential decay with a short component (T2 short) that represents 60% of the total sodium signal and a long component (T2 long) that represents 40% of the sodium signal. Due to the short T1 of sodium, rapid averaging can be used in sodium MRI in order to improve the SNR. However, the short T2 long (~12 ms) and the even shorter T2 short (~1 ms) result in significant loss of sodium signal when using conventional MR sequences with an echo time longer than 2 ms [11, 12]. Therefore, many recent studies on sodium MRI of articular cartilage at 7 T have used MR techniques with non-Cartesian k-space trajectories, such as 3D radial [13–17] or 3D cones [10], which enable ultra-short echo time (UTE) acquisition.

Madelin et al. applied compressed sensing to undersample a 3D radial UTE sequence for sodium MRI at 7 T [15]. These authors showed that compressed sensing can be applied to reduce the acquisition time by a factor of two at 7 T without losing sodium quantification accuracy. The nonlinear reconstruction used in compressed sensing can be used as an alternative to denoise fully sampled images. Parallel imaging techniques combined with sequences using non-Cartesian k-space trajectories at 7 T seem to be promising in further reducing the acquisition time of sodium MRI.

Staroswiecki et al. compared the sodium SNR at 3 and 7 T and verified that SNR scales linearly with field strength [10]. Sodium T2* values in patellar cartilage, measured with 3D cone trajectory, were not significantly different between 3 and 7 T and were consistent with previously reported relaxation times.

The sodium relaxation times in four different regions of the cartilage in the knee joint were measured in vivo on eight healthy volunteers at 7 T and reported by Madelin et al. [17]. The average sodium T1 was about 20 ms, but T2*short ranged from 0.5 to 1.4 ms and T2*long from 11.4 to 14.8 ms. Statistically significant differences in T1, T2*short, and T2*long were observed between the different regions in cartilage. Presented relaxation time measurements can be applied as correction factors for the calculation of sodium content in the articular cartilage.

Sodium MRI offers many potential clinical applications. Sodium content measured by $^{23}$Na MRI has been shown to be proportional to glycosaminoglycan (GAG) content in articular cartilage [18, 19]. Sodium MRI can be used to detect early signs of cartilage degeneration or injury before morphological changes can be detected by proton MRI [20]. Sodium MRI may enable the noninvasive in vivo evaluation of disease-modifying treatments for osteoarthritis (OA) and methods for cartilage repair. Affecting millions of people, OA is the most common degenerative disease of the musculoskeletal system.

In a study by Wang et al., cartilage sodium concentration in five healthy controls and five patients with OA was measured with 3D-radial UTE acquisition [13]. These

authors reported a statistically significant reduction in sodium concentration of 30–60% in OA patients when compared to healthy subjects. The findings are in good agreement with previous publications [11, 21] and suggest that sodium MRI at 7 T could be used for the detection of changes in cartilage associated with OA and may help to improve clinical diagnosis.

Because of thinness of cartilage, typically on the order of 3–5 mm, and the low resolution of sodium images, ROI evaluations are prone to partial volume errors, which could result in overestimation of sodium signal due to sodium signal from the synovial fluid. Madelin et al. addressed this issue by employing 3D radial UTE sodium sequences with fluid suppression and inversion recovery (IR) preparation of the magnetisation [14]. These investigators showed that a sequence with an adiabatic IR pulse generates a more uniform fluid suppression over the whole sample than a rectangular IR pulse, and therefore, can better separate sodium signal from the cartilage. Because of the specific absorption rate limits, the total acquisition time was about 17 min for the 3D radial sequence without IR or with the rectangular IR, and about 24 min for the adiabatic IR sequence.

Madelin et al. documented the reproducibility and repeatability of sodium quantification in cartilage in vivo by using a radial 3D sequence, with and without fluid suppression at 3 and 7 T [16]. These investigators did not observe any significant intermagnet, intersequence, intraday, or interday differences in the coefficients of variation. The reproducibility and repeatability were comparable to other proton-based MRI techniques for cartilage. Moreover, the fluid-suppressed sequence resulted in sodium concentrations (252 mM at 3 T; 278 mM at 7 T) that were closer to the values for healthy cartilage reported in the literature (220–310 mM) when compared to results from sequences without fluid suppression (171 mM at 3 T; 177 mM at 7 T). This difference was likely due to a reduction in partial volume errors from synovial fluid in sequences with fluid suppression.

The very short T2 times of sodium in articular cartilage result in sequences with short echo times that are very effective with regard to SNR. However, radial sequences are prone to blurring and artifacts from off-resonance effects, fast components of T2* decay, and variations in gradient timing. Although the Cartesian sampled sequences are less effective in regards to the SNR, they can offer much sharper images. In an article by Trattnig et al., a Cartesian 3D gradient echo sequence was used for sodium MRI at 7 T in patients after matrix-associated autologous chondrocyte transplantation (MACT) [22] (Fig. 1). These authors observed significant differences in sodium normalised values between repaired cartilage transplant tissue and healthy cartilage. Moreover, a strong significant correlation was found between sodium normalised values from 7 T and intravenously enhanced T1 values from another GAG-specific technique—delayed gadolinium-enhanced MRI of cartilage (dGEMRIC) at 3 T. These findings suggest that sodium MRI can differentiate between repaired tissue and native cartilage in MACT patients and may be useful for the noninvasive evaluation of different cartilage repair techniques.

### Sodium imaging of tendons

Degeneration of the Achilles tendon leads to thickening of the tendon [23]. Tendinopathy is also accompanied by disaggregation of the microfibrillar bundles due to the greater quantities of water and proteoglycan [24]. Almost double the GAG content was observed in pathologic tendons in studies using biochemical assays [25]. In a study by Juras et al., the feasibility of sodium magnetic resonance imaging for the diagnosis of Achilles tendinopathy was investigated at ultra-high field [26]. Their cohort comprised 20 healthy volunteers with no history of pain in the Achilles tendon and 8 patients with clinical findings of chronic Achilles tendinopathy. The study found that the mean bulk sodium SNR was 4.9±2.1 in healthy control subjects and 9.3±2.3 in patients with Achilles tendinopathy, and that the difference between the means was statistically significant. Figures 2 and 3 depict the increased sodium SNR in the tendinopathy group. This study not only showed a statistically significant increase in sodium SNR in patients with Achilles tendinopathy, compared with healthy tendons, but also revealed abnormal sodium signal values in the whole tendon, as well as morphologically focal abnormalities with focal thickening. Sodium signal values may correspond to GAG content in the Achilles tendon, which, as shown in in vitro studies, is increased with tendinopathy [26].

## T2* mapping of the Achilles tendon at 7 Tesla

MRI is quite frequently used to evaluate the Achilles tendon (AT). It was successfully employed to detect partial or total tendon rupture or even the degenerative processes in the tendon tissue. Most imaging findings are related to the pathologic processes of tendon degeneration and repair progression [27]. In addition to the morphological MRI evaluation (imaged predominantly by T2*-weighted sequences), the quantitative MRI analysis of tendon tissue may be helpful in identifying the early pathological changes in the tissue. Quantitative analysis of the relaxation or diffusion constants [such as T1, T2*, T1ρ, and apparent diffusion coefficient (ADC)] of the AT may provide additional information about the overall condition of the tendon. On conventional high-field MR systems (1.5–3 T), several parameters have been investigated as prospective markers

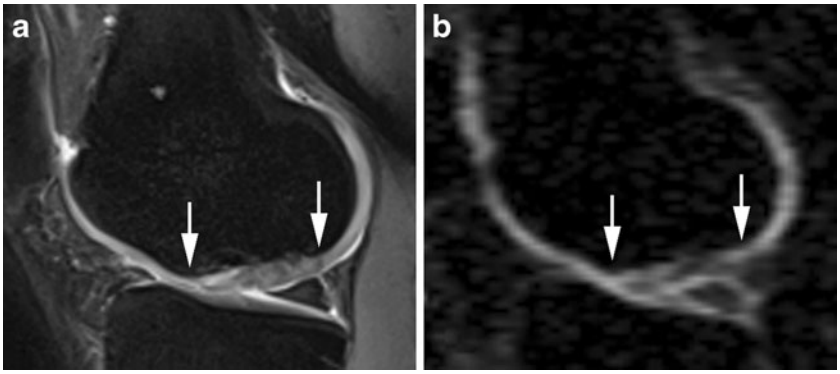


**Fig. 1** A proton-density-weighted image measured at 3 T (TR/TE=2,400/38 ms, resolution of 0.2×0.2×2.0 $mm^3$) (**a**) and a corresponding sodium image at 7 T (TR/TE=10/3.8 ms, resolution of 1.6×3.1×3.0 $mm^3$) (**b**) of a 23-year-old man, acquired 67 months after matrix-associated autologous chondrocyte transplantation (MACT) on the medial femoral condyle of the left knee. *Arrows* mark the borders of the transplanted area. The patient had a good outcome and MOCART score of 80 points. Please note lower intensity of sodium signal in repair area, which is suggestive of lower GAG content in the repair tissue than in surrounding native cartilage

for Achilles tendon degeneration, such as T2* [28], T1ρ [29], ADC [30], magnetisation transfer [31], or spectroscopically, even T2 [32]. Using spectroscopic methods, it was shown that the T2* decay in the Achilles tendon is a multicomponent process [33]. However, with clinical sequences, it is difficult to acquire signal from the second, third, and fourth components, since these have a small component ratio. The first component has the largest ratio, but it is in the submillisecond range, and thus, can barely be acquired with conventional echo times.

In general, MR imaging of rapidly relaxing tissues, such as tendons, menisci, ligaments, and bones, is rather difficult with clinical sequences. Recent developments in new hardware and sequence design allow the acquisition of a signal directly from these tissues. Moreover, ultra-high field provides a substantial increase in the SNR [9]. The 3D-UTE sequence provides the ability to detect MR signal from a large variety of rapidly relaxing tissues and materials, including tendons. Juras et al. used a 3D-UTE sequence at 7 T to estimate T2* in tendons in order to investigate the potential feasibility of using this parameter as a marker for Achilles tendinopathy [34]. The SNR increase between 3 and 7 T was validated by this study as well. Ten volunteers with no history of pain in the AT and five patients with chronic Achilles tendinopathy were recruited. T2* was acquired by fitting bi-component exponential functions, and both short (T2*s) and long (T2*l) were evaluated. With regard to the comparison of patients and volunteers at 7 T, the bulk T2*s was significantly higher in patients, although the bulk T2*l difference was not statistically significant. It seems that ultra-short bi-component T2* measurements in the human Achilles tendon in vivo are feasible using a 3D-UTE sequence. Higher SNR at 7 T allows the calculation of both T2* components very accurately. Figure 4 demonstrates a sample fit of signal intensities acquired by the 3D-UTE sequence. The observed differences between T2*s in healthy and abnormal tendons suggest that advanced quantitative imaging of the human AT may provide additional information beyond standard clinical imaging in reasonably short MR data acquisition times. T2* may be a promising marker for the diagnosis of early tendinopathy in the AT [34].

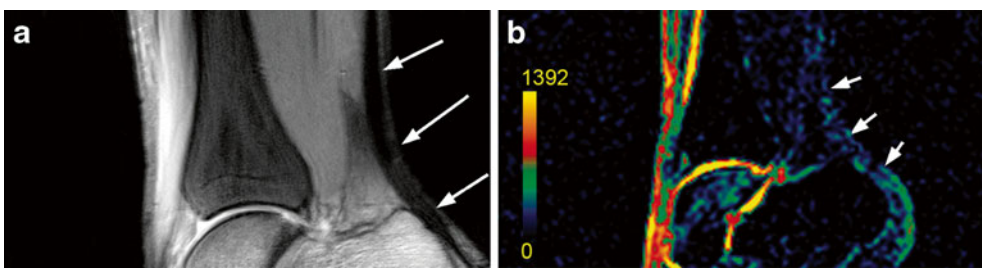


**Fig. 2** Magnetic resonance images from a 27-year-old healthy volunteer. **a** Proton-density-weighted turbo spin-echo (TSE) image with *arrows* pointing at the centers of each evaluated region of interest. Parameters: TR/TE 4,000/26 ms; field of view, 140×140; slice thickness, 3 mm. Please note that the Achilles tendon thickness and signal intensity are normal. **b** Corresponding 3D gradient-echo sodium (TR/TE 17/8.34 ms, field of view, 199×199; slice thickness, 3 mm) image depicts Achilles tendon sodium signal (*arrows*), which is relatively low. The *color bar* represents sodium signal intensity (courtesy of Medical University of Vienna)

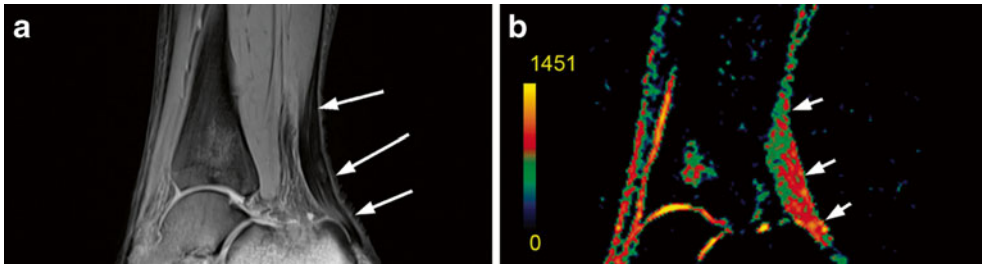


**Fig. 3** Magnetic resonance images of a 46-year-old patient with chronic Achilles tendinopathy. **a** Proton-density-weighted TSE image of the patient with chronic Achilles tendinopathy, with region-of-interest centers (*arrows*). **b** Corresponding color-coded 3D-gradient-echo sodium image depicts Achilles tendon sodium signal (*arrows*), which is obviously higher than that in the healthy volunteer. The sodium signal increase was observed in the whole tendon and not only in regions with clinical findings. *Color scale* represents sodium signal intensity values (courtesy of Medical University of Vienna)

## Chemical exchange saturation transfer (CEST) at 7 T

Saturation transfer (ST) is a commonly used technique in nuclear magnetic resonance (NMR) [35] and has been proposed as a method for the direct detection of chemical exchange between bulk water protons and protons bound to solutes [36]. The resultant MR imaging scheme is referred to as CEST MRI [37, 38]. The basic principle of CEST imaging is a reduction in bulk water MR signal after off-resonant spins are selectively pre-saturated by radiofrequency (RF) irradiation and then undergo chemical exchange with bulk water protons [39].

The hydroxyl and amide protons of glycosaminoglycans (GAG) provide exchange properties that render them principally suited for CEST experiments [40]. In vitro experiments at 11.7 T demonstrated that CEST imaging can be used as a biomarker for cartilage GAG content (gagCEST) in bovine cartilage samples [41, 42]. However, GAG –OH protons resonate at frequency offsets ($\Delta\omega$) of only 1 and 1.5–2 ppm downfield from bulk water, and rate constants of chemical exchange *(k)* can be on the order of 1,000 $s^{-1}$ [42]. At a magnetic field strength of 3.0 T, the $\Delta\omega$ of hydroxyl protons corresponds to a separation from bulk water of 128 Hz and 192–256 Hz in frequency units. As a consequence, radiofrequency power intended to selectively saturate –OH resonances simultaneously attenuates the bulk water signal (RF spillover), which impairs quantification of the CEST effect at 3.0 T. At higher fields, i.e., with increasing frequency differences, the RF spillover decreases, making ultra-high-field strengths, such as 7.0 T, ultimately favorable for CEST experiments.

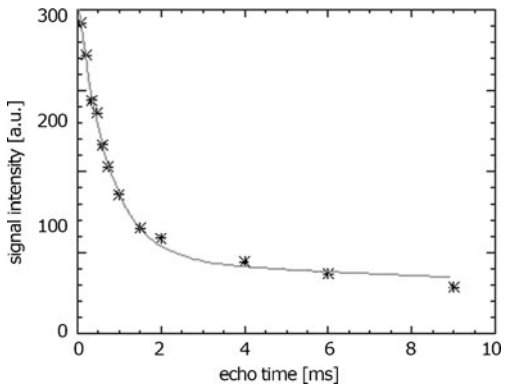


**Fig. 4** An example of the accuracy of bi-component T2* fitting in the Achilles tendon at 7 T (courtesy of Medical University of Vienna)

After the introduction of the gagCEST approach, further studies have been performed with animals and humans to assess the feasibility of gagCEST imaging in vivo [43–45], and several imaging sequences for fast and reliable detection of gagCEST effects have been proposed [43, 46–48]. Most techniques are based on multiple image acquisition with pre-saturation at different offset frequencies ($\Delta\omega$). The remaining bulk water signal ($M_{Sat}$), normalised to a reference ($M_{Ref}$), is then plotted against the RF presaturation offset (z-spectrum). CEST effects are asymmetric with respect to the water resonance, and thus, calculation of the asymmetry of the magnetisation transfer ratio (Eq. 1) ($MTR_{asym}(\Delta\omega) = (M_{Sat}(-\Delta\omega) - M_{Sat}(+\Delta\omega))/M_{Ref}$) provides a positive measure of CEST effects. Cartilage magnetisation transfer resonance asymmetry ($MTR_{asym}$) values scale linearly with the ratio of GAG protons to bulk water protons, given that temperature and pH values inside cartilage tissue are spatially equivalent within a sample, and $MTR_{asym}$ is evaluated at frequency offsets with underlying resonances of exchangeable GAG protons [42].

From the initial studies, the key requirements for in vivo gagCEST examinations can be derived: For accurate quantification of gagCEST effects, it is essential to account for inhomogeneities of the static magnetic field $B_0$ in a sample. For this purpose, fitting of the absorption curve and a separate reference MR data acquisition have been proposed as possible methods [43, 49, 50]. Furthermore, compensation for sample movement during the course of a measurement is crucial for accurate assignment of signal evolution to a certain location. Data from a separate $B_0$ reference also have to be aligned with the measurement data, which induces a greater registration effort.

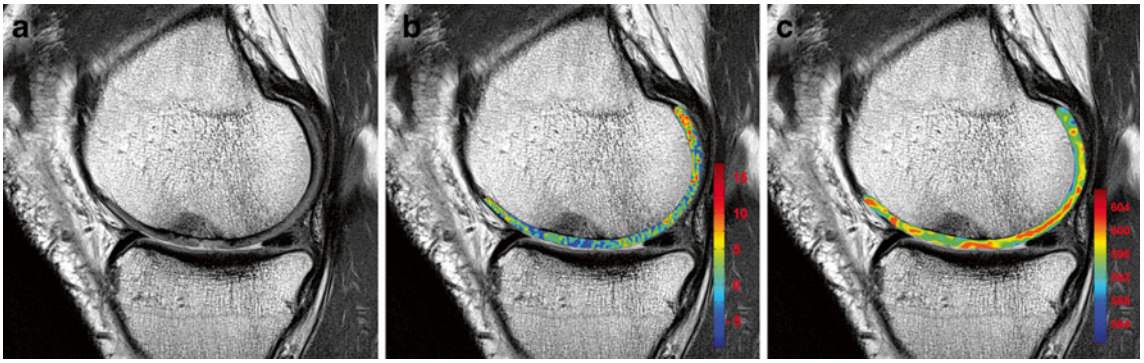


**Fig. 5** Sagittal knee images from a 49-year-old patient with a secondary cartilage defect after a tear of the anterior cruciate ligament. The central part of the lesion can be delineated in the morphologic proton-density-weighted image (**a**). The gagCEST (**b**) and sodium images (**c**) show a signal loss in the lesion compared to normal reference tissue. *Color bars* in **b** and **c** represent magnetisation transfer resonance asymmetry values summed over offsets from 0 to 1.3 ppm (gagCEST) and sodium signal-to-noise ratio, respectively

Despite the requirements mentioned above, gagCEST imaging is a valuable tool for the non-invasive assessment of GAG content in vivo. A recent study demonstrated that gagCEST can be used to reliably detect GAG in the knee cartilage of patients who had undergone cartilage repair surgery [51] (Fig. 5). This study was conducted at 7.0 T with a 3D GRE-based measurement technique, and $^{23}$Na MRI was used as a reference for GAG measurements. Moreover, the potential of gagCEST for GAG evaluation in intervertebral discs at 3.0 T has been demonstrated [52, 53]. Given the results from the latter studies, it seems possible that gagCEST can also be used to detect cartilage GAG content at 3 T, which indicates the potential of this approach for use in the clinical routine. The main strength of gagCEST compared to other GAG-sensitive imaging techniques, such as dGEMRIC and sodium imaging, is the relatively short acquisition time, which covers the entire volume of a knee joint in ~10 min [51], and gagCEST does not require administration of contrast agent and can easily be implemented into a standard imaging protocol.

## Metabolic imaging of muscles at 7 T

Another MR method that has the potential to become increasingly important in clinical musculoskeletal MR at 7 T is metabolic imaging or MR spectroscopy (MRS). MRS is a powerful noninvasive tool for the investigation of metabolite concentrations and studies of bioenergetics that could otherwise only be assessed by invasive muscle biopsies [54]. MRS provides information on a cellular level beyond the anatomical information assessed by standard imaging methods and aids in the understanding of various lesions [54–56], clinical diagnosis [56, 57], and treatment monitoring [58, 59].

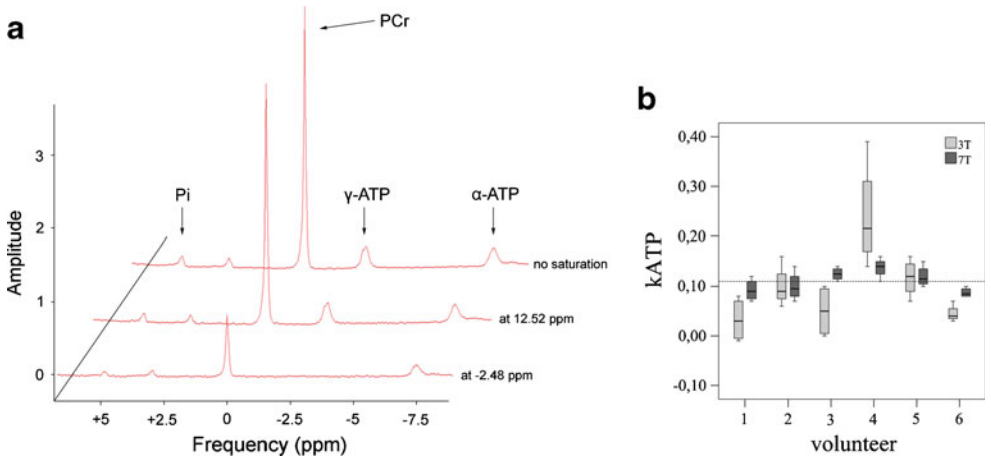


**Fig. 6** **a** Sample spectra with high spectral quality obtained in a total of 6 min by a magnetisation transfer experiment in the calf muscle of a healthy volunteer. To determine the forward rate constant of the ATPase reaction in the resting state accurately, it is necessary to acquire one spectrum with suppression of γ-ATP at −2.48 ppm and one spectrum with the suppression pulse set to 12.52 ppm (i.e., mirrored frequency position relative to Pi). **b** A box plot diagram illustrates the significantly higher intra- and intersubject reproducibility of measuring the time-resolved forward rate constant of the ATPase reaction (kATP) in the calf muscle of six healthy volunteers at 7 T compared to 3 T. For this assessment each subject was measured four times

The improvements in data quality for MRS techniques resulting from the higher B0 (i.e., 7 T) are larger than for standard MR imaging methods [60, 61]. In addition to SNR improvements, 7 T MRS also offers higher spectral resolution. SNR and spectral resolution together contribute to more reliable quantification of MRS data (i.e., more than three times higher than at 3 T [61, 62]) and enable a significantly more rapid acquisition time for MRS experiments [60, 62–64]. Based on the detected nuclei, MRS techniques can be classified as $^{1}$H-MRS, $^{31}$P-MRS, or $^{13}$C-MRS. Multinuclear MRS (i.e., $^{31}$P-MRS and $^{13}$C-MRS), in particular, improves significantly at 7 T [60, 62–66].

$^{1}$H-MRS provides insights into both lipid metabolism by quantification of intramyocellular (IMCL)/extramyocellular lipids (EMCL) [54, 67] and cancer metabolism by quantification of Cho compounds [68]. Recent reports on studies of lipid metabolism of the calf muscle at 7 T show more accurate and reliable results due to improved separation of individual IMCL and EMCL resonances by both 1D [69, 70] and 2D [70] correlated $^{1}$H-MRS. This can aid in clinical investigations of pathologic or training-related alterations in lipid muscle metabolism.

The $^{13}$C-MRS technique allows the in vivo measurement of glycogen, which is one of the major energy sources in the skeletal muscle besides IMCL/EMCL [71, 72]. One preliminary study at 7 T provides evidence of the significantly improved spectral quality along with a reproducibility that is more than three times better than that at 3 T [61]. Although $^{13}$C-MRS is not likely to enter clinical use, even with these improvements, $^{13}$C-MRS can nevertheless improve the understanding of pathological changes in glucose metabolism in muscle disease and could be applied in clinical trials that are designed to evaluate new drugs and therapies.

$^{31}$P-MRS is a popular tool that reveals the major factors of muscle metabolism noninvasively in a resting state and during muscle exercise [54, 62, 66, 73]. It allows the quantification of temporal changes in high-energy phosphates [66, 73], intracellular pH [54], and fluxes of creatine kinase and ATPase reactions [54, 62], which are important indicators of muscle metabolism. Several groups use $^{31}$P-MRS regularly for the investigation of muscle diseases in basic [57, 59, 74] and clinical [54, 56] research. In addition, $^{31}$P-MRS provides more specific markers of cancer metabolism than $^{1}$H-MRS [68].

In addition to SNR and spectral resolution improvements, T1 relaxation of $^{31}$P metabolites at 7 T is twice as fast as at 3 T (note that $^{31}$P is the only nucleus with decreasing T1) [60]. This improves the measurement speed, allowing acquisition of high quality data within a few minutes [60, 62–64] and improved spatial specificity [63, 64, 66]. In addition, at 7 T, there was an ~3 times higher reproducibility of $^{31}$P-MRS experiments than at 3 T [62] (Fig. 6). Apart from improved quantification of known metabolites, 7 T $^{31}$P-MRS might even be able to separately detect intramitochondrial inorganic phosphate pools [65].

The availability of fast and robust MRS methods at 7 T will provide new opportunities for imaging a large clinical spectrum of musculoskeletal diseases, such as mitochondrial disorders [75, 76], glycolytic defects [77], systemic diseases affecting muscle metabolism [56], muscle injury [78], or diabetes [74, 79], for diagnostic use [56, 57], therapy monitoring [58, 59], and clinical research [56].

In conclusion, these initial clinical studies demonstrate the potential of ultra-high-field MR at 7 T, with the advantage of significantly improved sensitivity for other nuclei, such as $^{23}$Na (sodium) and $^{31}$P (phosphorus). This will provide new insights into normal and abnormal physiology of musculoskeletal tissues and the metabolism of muscle, and will, therefore, provide new in vivo clinical applications.

**Acknowledgments** Funding for this study was provided by Vienna Spots of Excellence des Wiener Wissenschafts- und Technologie-Fonds (WWTF) and Vienna Advanced Imaging Center; grant sponsor: VIACLIC and the Slovak Scientific Grant Agency VEGA; grant number: 2/0090/11.

## References

1. Vaughan JT, Garwood M, Collins CM et al (2001) 7T vs. 4T: RF power, homogeneity, and signal-to-noise comparison in head images. Magn Reson Med 46:24–30
2. Ugurbil K, Adriany G, Andersen P et al (2003) Ultrahigh field magnetic resonance imaging and spectroscopy. Magn Reson Imaging 21:1263–1281
3. Tkac I, Andersen P, Adriany G et al (2001) In vivo 1H NMR spectroscopy of the human brain at 7T. Magn Reson Med 46:451–456
4. Yacoub E, Shmuel A, Pfeuffer J et al (2001) Imaging brain function in humans at 7 Tesla. Magn Reson Med 45:588–594
5. Pfeuffer J, Adriany G, Shmuel A et al (2002) Perfusion-based high-resolution functional imaging in the human brain at 7 Tesla. Magn Reson Med 47:903–911
6. Krug R, Carballido-Gamio J, Banerjee S et al (2008) In vivo ultra-high-field magnetic resonance imaging of trabecular bone microarchitecture at 7T. J Magn Reson Imaging 27:854–859
7. Nakada T, Matsuzawa H, Igarashi H et al (2008) In vivo visualization of senile-plaque-like pathology in Alzheimer's disease patients by MR microscopy on a 7T system. J Neuroimaging 18:125–129
8. van der Zwaag W, Francis S, Head K et al (2009) fMRI at 1.5, 3 and 7T: characterising BOLD signal changes. NeuroImage 47:1425–1434
9. Regatte RR, Schweitzer ME (2007) Ultra-high-field MRI of the musculoskeletal system at 7.0T. J Magn Reson Imaging 25:262–269
10. Staroswiecki E, Bangerter NK, Gurney PT et al (2010) In vivo sodium imaging of human patellar cartilage with a 3D cones sequence at 3T and 7T. J Magn Reson Imaging 32:446–451. doi:10.1002/jmri.22191

11. Borthakur A, Mellon E, Niyogi S et al (2006) Sodium and T1rho MRI for molecular and diagnostic imaging of articular cartilage. NMR Biomed 19:781–821
12. Borthakur A, Shapiro EM, Beers J et al (2000) Sensitivity of MRI to proteoglycan depletion in cartilage: comparison of sodium and proton MRI. Osteoarthr Cartil 8:288–293
13. Wang L, Wu Y, Chang G et al (2009) Rapid isotropic 3D-sodium MRI of the knee joint in vivo at 7T. J Magn Reson Imaging 30:606–614. doi:10.1002/jmri.21881
14. Madelin G, Lee JS, Inati S et al (2010) Sodium inversion recovery MRI of the knee joint in vivo at 7T. J Magn Reson 207:42–52. doi:10.1016/j.jmr.2010.08.003
15. Madelin G, Chang G, Otazo R et al (2011) Compressed sensing sodium MRI of cartilage at 7T: preliminary study. J Magn Reson. doi:10.1016/j.jmr.2011.12.005
16. Madelin G, Babb JS, Xia D et al (2011) Reproducibility and repeatability of quantitative sodium magnetic resonance imaging in vivo in articular cartilage at 3T and 7T. Magn Reson Med. doi:10.1002/mrm.23307
17. Madelin G, Jerschow A, Regatte RR (2011) Sodium relaxation times in the knee joint in vivo at 7T. NMR Biomed. doi:10.1002/nbm.1768
18. Wheaton AJ, Borthakur A, Shapiro EM et al (2004) Proteoglycan loss in human knee cartilage: quantitation with sodium MR imaging–feasibility study. Radiology 231:900–905
19. Shapiro EM, Borthakur A, Gougoutas A et al (2002) 23Na MRI accurately measures fixed charge density in articular cartilage. Magn Reson Med 47:284–291
20. Reddy R, Insko EK, Noyszewski EA et al (1998) Sodium MRI of human articular cartilage in vivo. Magn Reson Med 39:697–701
21. Shapiro EM, Borthakur A, Dandora R et al (2000) Sodium visibility and quantitation in intact bovine articular cartilage using high field (23)Na MRI and MRS. J Magn Reson 142:24–31
22. Trattnig S, Welsch GH, Juras V et al (2010) 23Na MR imaging at 7T after knee matrix-associated autologous chondrocyte transplantation preliminary results. Radiology 257:175–184
23. Schweitzer ME, Karasick D (2000) MR imaging of disorders of the Achilles tendon. AJR Am J Roentgenol 175:613–625
24. Samiric T, Parkinson J, Ilic MZ et al (2009) Changes in the composition of the extracellular matrix in patellar tendinopathy. Matrix Biol 28:230–236
25. Fu SC, Chan KM, Rolf CG (2007) Increased deposition of sulfated glycosaminoglycans in human patellar tendinopathy. Clin J Sport Med 17:129–134
26. Juras V, Zbyn S, Pressl C et al (2012) Sodium MR imaging of Achilles tendinopathy at 7T: preliminary results. Radiology 262:199–205
27. Gelberman RH, Manske PR, Vande Berg JS et al (1984) Flexor tendon repair in vitro: a comparative histologic study of the rabbit, chicken, dog, and monkey. J Orthop Res 2:39–48
28. Robson MD, Benjamin M, Gishen P et al (2004) Magnetic resonance imaging of the Achilles tendon using ultrashort TE (UTE) pulse sequences. Clin Radiol 59:727–735
29. Du J, Carl M, Diaz E et al (2010) Ultrashort TE T1rho (UTE T1rho) imaging of the Achilles tendon and meniscus. Magn Reson Med 64:834–842
30. Fechete R, Demco DE, Eliav U et al (2005) Self-diffusion anisotropy of water in sheep Achilles tendon. NMR Biomed 18:577–586
31. Hodgson RJ, Evans R, Wright P et al (2011) Quantitative magnetization transfer ultrashort echo time imaging of the Achilles tendon. Magn Reson Med 65:1372–1376
32. Henkelman RM, Stanisz GJ, Kim JK et al (1994) Anisotropy of NMR properties of tissues. Magn Reson Med 32:592–601
33. Peto S, Gillis P (1990) Fiber-to-field angle dependence of proton nuclear magnetic relaxation in collagen. Magn Reson Imaging 8:705–712
34. Juras V, Zbyn S, Pressl C et al (2012) Regional variations of T2* in healthy and pathologic achilles tendon in vivo at 7 Tesla: preliminary results. Magn Reson Med. doi:10.1002/mrm.24136
35. Forsen S, Hoffman RA (1963) Study of moderately rapid chemical exchange reactions by means of nuclear magnetic double resonance. J Chem Phys 39:2892
36. Guivel-Scharen V, Sinnwell T, Wolff SD et al (1998) Detection of proton chemical exchange between metabolites and water in biological tissues. J Magn Reson 133:36–45. doi:10.1006/jmre.1998.1440
37. Ward KM, Aletras AH, Balaban RS (2000) A new class of contrast agents for MRI based on proton chemical exchange dependent saturation transfer (CEST). J Magn Reson 143:79–87
38. Ward KM, Balaban RS (2000) Determination of pH using water protons and chemical exchange dependent saturation transfer (CEST). Magn Reson Med 44:799–802
39. Zhou JY, van Zijl PCM (2006) Chemical exchange saturation transfer imaging and spectroscopy. Prog Nucl Magn Reson Spectrosc 48:109–136
40. Ling W, Regatte RR, Schweitzer ME et al (2008) Characterization of bovine patellar cartilage by NMR. NMR Biomed 21:289–295
41. Ling W, Eliav U, Navon G et al (2008) Chemical exchange saturation transfer by intermolecular double-quantum coherence. J Magn Reson 194:29–32
42. Ling W, Regatte RR, Navon G et al (2008) Assessment of glycosaminoglycan concentration in vivo by chemical exchange-dependent saturation transfer (gagCEST). Proc Natl Acad Sci USA 105:2266–2270
43. Schmitt B, Bock M, Stieltjes B et al (2010) A new, 3D GRE based CEST imaging method for clinical application and verification with gagCEST in articular cartilage. In: Proceedings of the 18th Scientific Meeting, International Society for Magnetic Resonance in Medicine, Stockholm
44. Vinogradov E, Ivanishev A, Grant AK et al (2010) CEST and sodium imaging of glycosaminoglycans in-vivo in the 3T: preliminary results. In: Proceedings of the 18th Scientific Meeting, International Society for Magnetic Resonance in Medicine, Stockholm
45. Fenty M, Kassey V, Kogan F et al (2011) Feasibility of CEST imaging on the guinea pig stifle at 9.4T. In: Proceedings of the 19th Scientific Meeting, International Society for Magnetic Resonance in Medicine, Montreal
46. Vinogradov E, Lenkinski RE (2010) Detection of glycosaminoglycans using positive CEST approach. In: Proceedings of the 18th Scientific Meeting, International Society for Magnetic Resonance in Medicine, Stockholm
47. Varma G, Alsop DC, Lenkinski RE et al (2011) Optimization of pulsed-gagCEST at 3.0T. In: Proceedings of the 19th Scientific Meeting, International Society for Magnetic Resonance in Medicine, Montreal
48. Varma G, Lenkinski RE, Vinogradov E (2011) Keyhole chemical exchange saturation transfer. In: Proceedings of the 19th Scientific Meeting, International Society for Magnetic Resonance in Medicine, Montreal
49. Kim M, Chan Q, Anthony MP et al (2010) Assessment of glycosaminoglycan distribution in human lumbar intervertebral discs using chemical exchange saturation transfer. In: Proceedings of the 18th Scientific Meeting, International Society for Magnetic Resonance in Medicine, Stockholm
50. Wei W, Jia G, Flanigan DC et al (2011) Examining the accuracy of dual echo B0 map for field inhomgeneity correction with the application of gagCEST in articular cartilage at 3T. In: Proceedings of the 19th Scientific Meeting, International Society for Magnetic Resonance in Medicine, Montreal
51. Schmitt B, Zbyn S, Stelzeneder D et al (2011) Cartilage quality assessment by using glycosaminoglycan chemical exchange

saturation transfer and (23)Na MR imaging at 7T. Radiology 260:257–264
52. Ling W, Saar G, Regatte R et al (2009) Assessing the intervertebral disc via gagCEST. In: Proceedings of the 17th Scientific Meeting, International Society for Magnetic Resonance in Medicine, Honolulu
53. Kim M, Chan Q, Anthony MP et al (2011) Assessment of glycosaminoglycan distribution in human lumbar intervertebral discs using chemical exchange saturation transfer at 3T: feasibility and initial experience. NMR Biomed 24:1137–1144
54. Boesch C (2007) Musculoskeletal spectroscopy. J Magn Reson Imaging 25:321–338
55. Lindquist D (2008) What can 31P MR spectroscopy tell us about muscle disease? Radiology 247:1–2
56. Taylor DJ (2000) Clinical utility of muscle MR spectroscopy. Semin Musculoskelet Radiol 4:481–502
57. Ko SF, Huang CC, Hsieh MJ et al (2008) 31P MR spectroscopic assessment of muscle in patients with myasthenia gravis before and after thymectomy: initial experience. Radiology 247:162–169
58. Taivassalo T, Matthews PM, DeStefano N et al (1996) Combined aerobic training and dichloroacetate improve exercise capacity and indices of aerobic metabolism in muscle cytochrome oxidase deficiency. Neurology 47:529–534
59. Lodi R, Hart PE, Rajagopalan B et al (2001) Antioxidant treatment improves in vivo cardiac and skeletal muscle bioenergetics in patients with Friedreich's ataxia. Ann Neurol 49:590–596
60. Bogner W, Chmelik M, Schmid AI et al (2009) Assessment of P-31 relaxation times in the human calf muscle: a comparison between 3T and 7T in vivo. Magn Reson Med 62:574–582
61. Stephenson MC, Frances G, Napolitano A et al (2011) Applications of multi-nuclear magnetic resonance spectroscopy at 7T. World J Radiol 3:105–113
62. Valkovič L, Chmelík M, Just-Kukurova I et al (2011) Time-resolved phosphorous magnetization transfer of the human calf muscle at 3T and 7T: a feasibility study. Eur J Radiol. doi:10.1016/j.ejrad.2011.09.024,
63. Bogner W, Chmelik M, Andronesi OC et al (2011) In vivo (31)P spectroscopy by fully adiabatic extended image selected in vivo spectroscopy: a comparison between 3T and 7T. Magn Reson Med 66:923–930
64. Chmelík M, Just-Kukurová I, Gruber S et al (2012) Fully adiabatic 31P 2D-CSI with reduced chemical shift displacement error at 7T – GOIA-1D-ISIS/2D-CSI – goISICS. Magn Reson Med (in press)
65. Kan HE, Klomp DWJ, Wong CS et al (2010) In vivo (31)P MRS detection of an alkaline inorganic phosphate pool with short T1 in human resting skeletal muscle. NMR Biomed 23:995–1000
66. Meyerspeer M, Scheenen T, Schmid AI et al (2011) Semi-LASER localized dynamic (31)P magnetic resonance spectroscopy in exercising muscle at ultra-high magnetic field. Magn Reson Med 65:1207–1215
67. Krssak M, Petersen KF, Dresner A et al (1999) Intramyocellular lipid concentrations are correlated with insulin sensitivity in humans: a H-1 NMR spectroscopy study. Diabetologia 42:113–116
68. Negendank W (1992) Studies of human tumors by MRS—a review. NMR Biomed 5:303–324
69. Khuu A, Ren J, Dimitrov I et al (2009) Orientation of lipid strands in the extracellular compartment of muscle: effect on quantitation of intramyocellular lipids. Magn Reson Med 61:16–21
70. Ramadan S, Ratai EM, Wald LL et al (2010) In vivo 1D and 2D correlation MR spectroscopy of the soleus muscle at 7T. J Magn Reson 204:91–98
71. Taylor R, Price TB, Rothman DL et al (1992) Validation of C-13 NMR measurement of human skeletal-muscle glycogen by direct biochemical assay of needle-biopsy samples. Magn Reson Med 27:13–20
72. Krssak M, Petersen KF, Bergeron R et al (2000) Intramuscular glycogen and intramyocellular lipid utilization during prolonged exercise and recovery in man: a (13)C and (1)H nuclear magnetic resonance spectroscopy study. J Clin Endocrinol Metab 85:748–754
73. Prompers JJ, Jeneson JAL, Drost MR et al (2006) Dynamic MRS and MRI of skeletal muscle function and biomechanics. NMR Biomed 19:927–953
74. Szendroedi J, Schmid AI, Meyerspeer M et al (2009) Impaired mitochondrial function and insulin resistance of skeletal muscle in mitochondrial diabetes. Diabetes Care 32:677–679
75. Kuhl CK, Layer G, Traber F et al (1994) Mitochondrial encephalomyopathy—correlation of P-31 exercise MR spectroscopy with clinical findings. Radiology 192:223–230
76. Taylor DJ, Kemp GJ, Radda GK (1994) Bioenergetics of skeletal-muscle in mitochondrial myopathy. J Neurol Sci 127:198–206
77. Duboc D, Jehenson P, Dinh ST et al (1987) Phosphorus NMR-spectroscopy study of muscular enzyme deficiencies involving glycogenolysis and glycolysis. Neurology 37:663–671
78. Mccully KK, Argov Z, Boden BP et al (1988) Detection of muscle injury in humans with 31-P magnetic-resonance spectroscopy. Muscle Nerve 11:212–216
79. Phielix E, Mensink M (2008) Type 2 diabetes mellitus and skeletal muscle metabolic function. Physiol Behav 94:252–258